Black carbon solar absorption suppresses turbulence in the atmospheric boundary layer

Eric M. Wilcox[a,1], Rick M. Thomas[b,c,1], Puppala S. Praveen[b,d], Kristina Pistone[b,e], Frida A.-M. Bender[f,g], and Veerabhadran Ramanathan[b,1]

[a]Division of Atmospheric Sciences, Desert Research Institute, Reno, NV 89512; [b]Center for Clouds, Chemistry and Climate, Scripps Institution of Oceanography, University of California, San Diego, La Jolla, CA 92093; [c]School of Geography, Earth and Environmental Sciences, University of Birmingham, Birmingham B15 2TT, United Kingdom; [d]International Centre for Integrated Mountain Development, Kathmandu, Nepal; [e]Ames Research Center, Universities Space Research Association, National Aeronautics and Space Administration (NASA), Moffett Field, CA 94035; [f]Department of Meteorology, Stockholm University, 106 91 Stockholm, Sweden; and [g]Bolin Centre for Climate Research, Stockholm University, 106 91 Stockholm, Sweden

Edited by Mark H. Thiemens, University of California, San Diego, La Jolla, CA, and approved August 26, 2016 (received for review December 31, 2015)

The introduction of cloud condensation nuclei and radiative heating by sunlight-absorbing aerosols can modify the thickness and coverage of low clouds, yielding significant radiative forcing of climate. The magnitude and sign of changes in cloud coverage and depth in response to changing aerosols are impacted by turbulent dynamics of the cloudy atmosphere, but integrated measurements of aerosol solar absorption and turbulent fluxes have not been reported thus far. Here we report such integrated measurements made from unmanned aerial vehicles (UAVs) during the CARDEX (Cloud Aerosol Radiative Forcing and Dynamics Experiment) investigation conducted over the northern Indian Ocean. The UAV and surface data reveal a reduction in turbulent kinetic energy in the surface mixed layer at the base of the atmosphere concurrent with an increase in absorbing black carbon aerosols. Polluted conditions coincide with a warmer and shallower surface mixed layer because of aerosol radiative heating and reduced turbulence. The polluted surface mixed layer was also observed to be more humid with higher relative humidity. Greater humidity enhances cloud development, as evidenced by polluted clouds that penetrate higher above the top of the surface mixed layer. Reduced entrainment of dry air into the surface layer from above the inversion capping the surface mixed layer, due to weaker turbulence, may contribute to higher relative humidity in the surface layer during polluted conditions. Measurements of turbulence are important for studies of aerosol effects on clouds. Moreover, reduced turbulence can exacerbate both the human health impacts of high concentrations of fine particles and conditions favorable for low-visibility fog events.

atmospheric turbulence | cloud cover | aerosols | radiative forcing | autonomous unmanned aerial vehicles

Black carbon (BC) aerosols associated with the outflow of soot pollution from South Asia spread broadly across the northern Indian Ocean during the winter monsoon season (1). These BC aerosols directly heat the atmosphere because of absorption of solar radiation (2), and also instantaneously increase the albedo of the clouds (3) from the Twomey effect (4). Both processes reduce the amount of sunlight reaching the surface, causing a surface cooling of climate. However, changes in low cloud cover, if caused by aerosols, have perhaps the greatest impact on the net radiative effect of aerosols in this region. Whereas the Twomey effect has been argued to result in an increase in cloud cover (5), the response of turbulence in the boundary layer may play an important role in determining whether aerosol effects result in an increase or a decrease in cloudiness (6, 7).

The aerosol absorption in this region is thought to "burn off" the clouds by reducing the relative humidity in the cloud layer and suppressing convection, thereby causing a warming of climate by allowing more sunlight to penetrate to the surface (8). A reduction in low cloudiness is not always the response to lower-tropospheric heating by absorbing soot and smoke aerosols, however. If the heating reduces turbulent entrainment of dry air from above the humid marine boundary layer, then a thicker layer of clouds can be supported by the greater relative humidity in the surface mixed layer (9, 10). The result is an enhancement of cloud albedo and a reduction in absorbed solar radiation that partly compensates for the increase in net radiative forcing attributable to the dark aerosol residing above a bright cloudy scene (11). Thus, the conceptual view has emerged that BC aerosols within the cloud layer tend to reduce clouds, leading to climate warming, whereas BC aerosols above the cloud layer tend to increase clouds, leading to climate cooling (12). Previous studies have not directly observed the relationship between BC aerosols in the atmosphere and turbulence in the boundary layer, however. Here we used such measurements to demonstrate how BC aerosols within the cloud layer may reduce turbulence and enhance relative humidity in the cloudy surface mixed layer.

The CARDEX Campaign

We examined the links among BC, its solar absorption, and vertical profiles of turbulent fluxes within the boundary layer to understand how the response of turbulence to aerosol forcing impacts clouds. The central component of the Cloud Aerosol Radiative Forcing and Dynamics Experiment (CARDEX) (13) was the deployment of lightweight unmanned aerial vehicles (UAVs) for aerosol, radiation, cloud, and turbulent flux measurements (3, 14, 15), advancing the procedures developed in previous UAV studies (2, 3). The field study was conducted at the Maldives Climate Observatory–Hanimaadhoo (MCOH) (1) during February and March 2012. The existing long-term aerosol and radiation measurements at the observatory were augmented with the UAV aerosol, cloud, and turbulence sampling measurements, as well as micropulse lidar

Significance

The cooling effect of aerosols on climate and the modification of clouds by aerosols have been widely debated, because quantifying their effects is important for constraining current climate change. Here we present measurements of turbulence from unmanned aerial vehicles. We find that absorption of sunlight by black carbon (BC) aerosols suppresses turbulence in the lower atmosphere, with important consequences for the environmental impacts of BC emissions from anthropogenic fossil fuel and biomass burning. A mechanism is proposed that links the suppressed turbulence to taller clouds. These results highlight the importance of understanding and observing the role of turbulence in studies of aerosol impacts on clouds. Suppressed turbulence also exacerbates the visibility and human health impacts of pollution.

Author contributions: E.M.W., R.M.T., P.S.P., K.P., F.A.-M.B., and V.R. designed research; E.M.W., R.M.T., P.S.P., K.P., F.A.-M.B., and V.R. performed research; E.M.W., R.M.T., P.S.P., K.P., and F.A.-M.B. analyzed data; and E.M.W., R.M.T., and K.P. wrote the paper.

The authors declare no conflict of interest.

This article is a PNAS Direct Submission.

[1]To whom correspondence may be addressed. Email: Eric.Wilcox@dri.edu; r.thomas@bham.ac.uk; or vramanathan@ucsd.edu.

data, microwave radiometry data, and high-frequency wind measurements for near-surface turbulence. The microwave radiometry and near-surface turbulence measurements were made from the top of a 15-m-tall tower.

Profiles of the turbulent kinetic energy (TKE) and vertical flux of latent heat were obtained during near-daily UAV flights in order to study their role in aerosol impacts on clouds and climate. The UAV turbulence measurement system was previously compared with stationary measurements comparable to the tower measurements from MCOH and demonstrated errors of at most 5% (15). During CARDEX, UAV turbulence data were calculated from subsections of 10- to 15-km horizontal flight legs. Subsection lengths were typically 9.5 km and were determined postflight for each flight as those that captured the full spectral range in covariance ogives and displayed a minimum in wind component variances. At 12–16 times the surface mixed layer height (~600–800 m), 9.5 km is within the range previously suggested as required to constrain the accuracy of turbulent variations to within 10% (16).

The tower measurements of turbulence at MCOH were obtained with a Gill WindMaster Pro sonic anemometer and a Campbell Krypton hygrometer mounted on a mast extending to 23 m above the surface. Water vapor fluctuations and 3D wind vectors were logged at 20 Hz for the derivation of sensible heat, TKE, and water vapor fluxes using eddy covariance methods (17). TKE was calculated based on all three components of wind velocity. Data processing was performed in 30-min averaging periods with despiking to remove points >3σ of a running 60-s mean, and linear detrending was applied. The tower is <75 m from the ocean on the northern side of the island, and only data from this wind direction were included in the final analysis.

Profiles of the aerosol absorption coefficient and BC aerosol concentration were determined using a miniaturized version of a three-wavelength absorption photometer (14). Level flights of 5- to 10-min duration are required to reduce random error in the absorption photometer. The BC concentration was determined based on the absorption coefficient at 870 nm using an absorption cross-section of 10 m^2 g^{-1}. UAV measurements of absorption coefficient in the surface mixed layer agree to within 10% with simultaneous surface measurements made with a commercial aethalometer (14).

The aircraft outfitted with aerosol sampling instruments routinely performed profiles up to an altitude of 3 km, from which the profiles of equivalent potential temperature were derived. Level flights at selected heights between 500 m and 3 km were then performed to construct the absorption coefficient and BC aerosol concentration profiles. Profiles from 7 d of flight were included in the polluted profiles (N_a at MCOH >1,500 cm^{-3}), and profiles from four flight days were included in the cleaner profiles (N_a at MCOH <1,000 cm^{-3}).

The atmospheric boundary layer height was determined using the MiniMPL micro pulse lidar (Sigma Space) (18). To distinguish aerosol features confined to the surface mixed layer from elevated aerosol plumes, an upper bound was imposed on the automated algorithm based on subjective analysis of the backscatter profiles ranging from 900 m to 1,700 m, depending on the day.

Results

During the winter monsoon, there is a well-mixed atmospheric layer above the northern Indian Ocean, referred to here as the surface mixed layer, which extends from the ocean surface to a strong capping inversion at the top of the surface layer below 1 km altitude. At the top of the surface mixed layer, the potential temperature increases by 2 K or more in 100 m of vertical distance, and the relative humidity decreases from ~75% within the surface mixed layer to ~50% on average (and often much lower) in the drier layer above. The bases of small cumulus clouds reside at the top of the surface mixed layer and penetrate into the inversion, as is typical for trade wind cumulus cloud regions; however, in many such locations, the

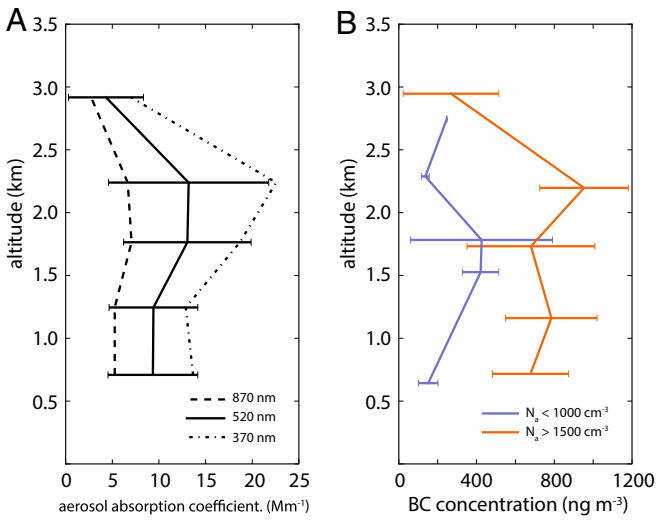

Fig. 1. Profiles of the aerosol absorption coefficient at three wavelengths (*A*) and black carbon (BC) aerosol mass concentration (*B*). Blue lines denote profiles when aerosol particle concentration (particles with diameters between 10 nm and 10 μm; denoted N_a) at MCOH is <1,000 cm^{-3}. Orange lines are for aerosol particle concentration at MCOH >1,500 cm^{-3}. Horizontal bars represent 1 SD at each altitude level. Profiles are averages of UAV profiles from 7 d of the more polluted condition and 4 d of the less polluted condition.

cloud tops range from just above the top of the surface mixed layer to as high as 3 km where a weaker temperature inversion, known as the trade wind inversion, occurs (19). In contrast, the dry stable layer above the capping inversion prevents the weak cumulus clouds over the northern Indian Ocean from penetrating much further above the inversion at the top of the surface mixed layer, and the cloud fraction is typically <0.1.

The mean profile of the aerosol absorption coefficient peaked at an altitude of ~2 km (Fig. 1*A*). The soot layer containing the BC aerosol extended from the surface up to an altitude of 3 km on average, although there was considerable daily variability in the structure of the profile. Pollution occurs more frequently above 1,500 m altitude when the origin of the lower-tropospheric flow is over the continent, and the particle concentration at the surface often increases during these periods as well (14). Through the dry winter monsoon season, the increase in surface pollution is indicative of transport in the column up to 3 km (1). This increase in aerosol optical depth (AOD) coincides with an increase in the absorption coefficient and a decrease in aerosol single-scattering albedo (1), attributed to continental pollution characterized by high concentrations of submicron light-absorbing aerosol (20).

The BC aerosol concentration profiles from 11 d of flights were sorted according to particle concentration measurements at the surface. These profiles show that the BC concentration was significantly greater up to 3 km altitude with increased pollution at the surface (Fig. 1*B*). The mean absorption coefficient at 2 km shown in Fig. 1 is of comparable magnitude to the profile reported during the polluted episode of the previous Maldives Airborne Campaign (MAC) (2, 14), but substantially larger in the atmospheric boundary layer below 1.5 km compared with that of the MAC. The diurnally averaged solar heating rate of the atmosphere at 2 km altitude was estimated as nearly 1 K d^{-1} based on direct observations of the convergence of solar flux between stacked UAVs during the MAC polluted period (2). Thus, the average aerosol heating rate during the CARDEX campaign was likely comparable during polluted episodes. Aerosol heating within the surface mixed layer may be greater than the ~0.2 K d^{-1} estimated during the MAC polluted episode because of the greater absorption coefficient in the surface mixed layer during CARDEX. During the Indian Ocean

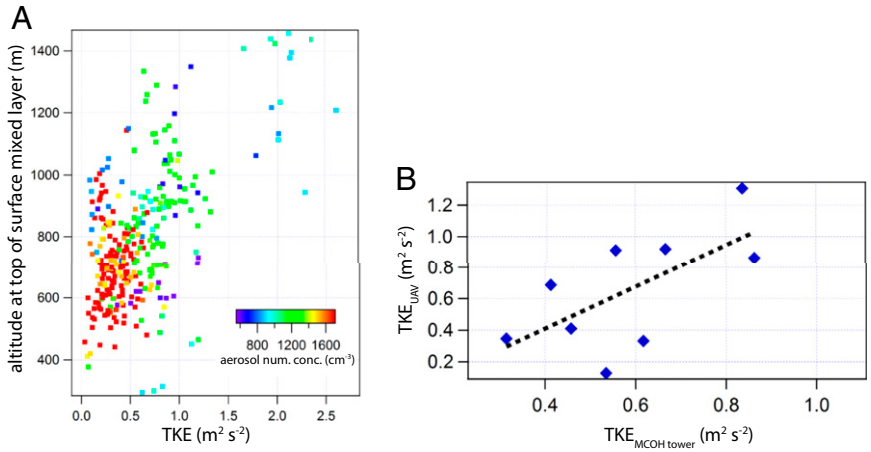

Fig. 2. (*A*) Altitude at the top of the surface mixed layer estimated from the gradient in micropulse lidar backscatter against TKE measured at the top of the 15-m tower at MCOH. Each sample is colored according to the aerosol particle concentration (particles with diameters between 10 nm and 10 μm) at MCOH. (*B*) TKE measured by UAV in the upper part of the atmospheric boundary layer against a simultaneous measurement at the MCOH tower.

Experiment (INDOEX), solar absorption in the aerosol layer was estimated to cause a reduction in surface solar flux of −18 W m^{-2}, with aerosol scattering causing an additional reduction of −2 W m^{-2} at the surface (21). Thus, the northern Indian Ocean is characterized by a deep layer of BC aerosols contributing heating from within the surface mixed layer to an altitude of up to 3 km. Shallow cumulus clouds are embedded within the BC aerosol layer (3, 22).

The TKE and height of the top of the surface mixed layer are shown in Fig. 2*A* as a scatterplot where the color of the points indicates the particle concentration near the surface. As pollution increased at MCOH (indicated by yellow and red colored samples), TKE decreased. A reduction in TKE inhibits the upward mixing of the surface mixed layer top by entrainment of dry air from above the inversion into the surface layer. Therefore, the altitude of the surface mixed layer top was lower during the polluted periods of decreased TKE. In addition to the surface measurements, TKE was profiled through the surface mixed layer by UAV. We find that TKE above the surface and in the surface mixed layer roughly correlates with surface measurements of TKE (Fig. 2*B*), suggesting that the reduced turbulence during polluted conditions extends through this layer.

The inversion capping the surface mixed layer is characterized by a decrease in equivalent potential temperature (θ_e) above the surface layer with nearly uniform θ_e (solid lines in Fig. 3*A*). The polluted conditions during CARDEX coincided with a lower capping inversion at ∼600 m altitude (orange solid line in Fig. 3*A*) compared with ∼800 m altitude during cleaner conditions (blue solid line in Fig. 3*A*), consistent with the lower boundary layer top altitude indicated by the micropulse lidar in Fig. 2*A*.

Polluted conditions also corresponded to a warmer and more humid surface mixed layer, as indicated by a greater θ_e value compared with that in cleaner conditions. Boundary layer temperature was greater by ∼1 K during polluted conditions compared with cleaner conditions and the mean surface relative humidity increased from 69.7% during cleaner conditions to 77.4% during polluted conditions. Despite the lower altitude of the surface mixed layer top during polluted conditions, the layer of nearly saturated air conducive to cloud formation (where $\theta_e = \theta_{es}$) was thicker during more polluted conditions compared with less polluted conditions. Multiyear observations of cloud top heights from the National Aeronautics and Space Administration's Cloud-Aerosol Lidar with Orthogonal Polarization (CALIOP) satellite lidar confirm that cloud tops were almost uniformly confined to within a few hundred meters of the surface mixed layer top (Fig. 3*B*). The CALIOP vertical feature mask (version 3) (23, 24) profiles were sorted according to multiyear observations of AOD from the moderate-resolution imaging spectroradiometer (MODIS) to separate the number of observed cloud tops when AOD was below the median value over MCOH (0.3) from the number of cloud tops when AOD exceeded the median value. Approximately 100 overpasses of the CALIOP instrument are included here, representing every overpass within ∼250 km of MCOH during February and March in 2007–2013.

Regardless of the amount of aerosol, most of the cloud tops were found between 400 m and 1,200 m, with the peak occurrence at 600–700 m. Despite the reduced turbulence and lowered top of the surface mixed layer by at least 200 m, the altitude of the cloud tops was similar in the less polluted and more polluted conditions.

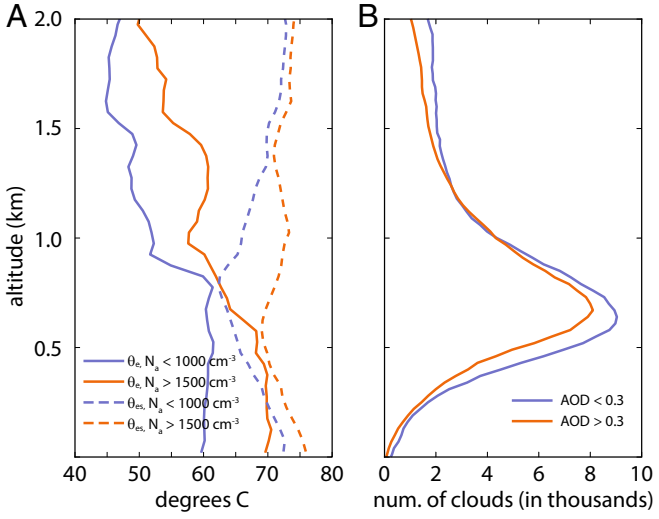

Fig. 3. (*A*) Profiles of equivalent potential temperature (solid lines) and saturated equivalent potential temperature (dashed lines) measured by UAV. These profiles are averages of the same flights shown in Fig. 1. Blue lines denote profiles when aerosol particle concentration (particles with diameters between 10 nm and 10 μm denoted as N_a) at MCOH is <1,000 cm^{-3}. Orange lines are for aerosol particle concentrations at MCOH >1,500 cm^{-3}. (*B*) Number of cloud features observed by the CALIOP lidar on the Calipso satellite. Data are from all passes of Calipso during February 2007–2013 and all samples within 5° latitude/longitude of MCOH. The blue line denotes profiles where the AOD is <0.3 (the median value) observed by the MODIS instrument on the Aqua satellite flying in formation with the CALIOP observations. The orange line denotes profiles where the AOD is >0.3.

Table 1. Linear regression analysis of daytime relative humidity at 1,000 hPa with dynamical parameters in the February and March 2006–2012 ECMWF ERA-Interim reanalysis at the model grid cell corresponding to the MCOH station

Reanalysis parameter	Correlation with relative humidity at 1,000 hPa	Correlation with surface particle concentration	Difference between N_a >1,500 cm^{-3} and N_a <1,000 cm^{-3}
Vertical velocity at 925 hPa	−0.30	−0.05	−0.012 Pa s^{-1}
Vertical velocity at 750 hPa	−0.25	0.05	−0.013 Pa s^{-1}
Zonal velocity at 750 hPa	−0.21	−0.07	−0.87 m s^{-1}
Divergence at 1,000 hPa	−0.21	−0.18	-3.0×10^{-6} s^{-1}
Divergence at 750 hPa	−0.07	−0.12	-3.7×10^{-7} s^{-1}
Zonal velocity at 1,000 hPa	−0.05		
Meridional velocity at 750 hPa	0.02		
Meridional velocity at 1,000 hPa	0.01		
Potential temperature difference, 750 hPa − 1,000 hPa	0.03		
Geopotential at 500 hPa	0.07		

Correlation coefficients (*r*) are shown with the sign of the relationship. Correlations of dynamical parameters with surface particle concentration (N_a) and differences between more polluted and less polluted conditions are based on particle concentration measurements from the 2006 and 2012 seasons.

During the cleaner conditions, clouds did not have sufficient buoyancy to penetrate the inversion, and CALIOP showed that most of the cumulus cloud tops were below the elevation of the inversion observed during CARDEX. In contrast, during polluted conditions, most of the cloud tops were above the elevation of the inversion, indicating greater vertical cloud development allowed by the more humid polluted conditions. Although the CALIOP data are from a multiyear climatology, the foregoing findings are consistent with a companion study showing an increasing cloud liquid water path with increasing aerosol for clouds observed with a ground-based microwave radiometer during the CARDEX period (25). Both the CALIOP result and the microwave radiometry results are consistent with the thicker saturated layer under more polluted conditions shown in Fig. 3*B*.

Discussion

The conceptual picture that emerges from the foregoing observations is one in which aerosol absorption heats the boundary layer and lower troposphere under polluted conditions. A reduction in boundary layer TKE decreases the entrainment of air across the temperature inversion at the top of the boundary layer, which favors a lower surface mixed layer top. The reduced turbulence might initially suppress cloud development; however, the reduced turbulent mixing across the inversion also leads to greater relative humidity in the surface mixed layer because of weakened mixing of moist air up through the interface and weakened mixing of dry tropospheric air down into the mixed layer. Thus, the vertical profile shifts from a condition in which clouds are confined to the top of the surface mixed layer to a condition in which clouds form in a thicker saturated layer and may penetrate above the inversion, because greater humidity provides additional buoyancy.

Large-eddy simulations of the response of northern Indian Ocean cumulus clouds to heating by absorbing aerosols previously indicated that heating within the cloud layer can reduce relative humidity and low cloud cover, thereby contributing a positive semidirect radiative heating during the winter monsoon (8). Long-term records of low clouds suggest that a slight increase in cloud cover occurred over the northern Indian Ocean during a time when aerosol emissions were increasing (26). Remote sensing data suggest that low cloud cover increases with increasing aerosol optical thickness for small amounts of aerosol and decreases with increasing aerosol optical thickness for large amounts of aerosol (27, 28). Thus, the response of low clouds to BC aerosol absorption may depend on the amount of aerosol present. Enhancement of cloud development and lowering of the boundary layer top owing to aerosol heating above clouds has been observed over the southeastern Atlantic Ocean (10). Although the consequences of BC absorption for the coverage of clouds was not measured during CARDEX, the enhanced humidity and thicker saturated cloud layer observed during the more polluted conditions of CARDEX suggest that the same process may impact trade cumulus clouds within a layer of absorbing aerosol, as was observed for southeastern Atlantic clouds beneath absorbing aerosols, at least for the conditions seen during CARDEX.

The consequences of BC aerosols for radiative forcing of climate depend on the balance among direct aerosol radiative heating, increases in cloud drop concentration (3, 22), and the changes in turbulence and relative humidity described here. Further study is needed to account for the full range of variability in BC aerosol loading and the combined radiative effects of changes in cloud microphysics, changes in cloud development in response to reduced turbulence, and changes in cloud cover with increasing aerosol.

The observations available from CARDEX are suggestive of a mechanism by which absorbing aerosols can lead to increased humidity rather than decreased humidity in the surface mixed layer where cumulus cloud updrafts originate. We note that such relationships among observed aerosol amounts, TKE, humidity, and temperature are not on their own sufficient to rule out the possibility that the atmospheric dynamics leading to increasing aerosol also leads to a warmer and more humid surface mixed layer independent of the aerosols. Further modeling experiments are certainly warranted to isolate the impact of aerosols from these additional factors. We note that heating of the aerosol layer by BC aerosol absorption has been measured directly and independently of meteorological influence (2), and also that the more polluted air masses have their origin over the continent, whereas the less polluted air masses originate over the ocean (29). Based on air mass history, one might expect that more polluted air masses would be warmer and drier than the less polluted air masses. Our proposed mechanism explains why the expected result is not what was observed, and also why the expected reduction in cloud cover due to BC aerosols was not apparent in previous studies of remote sensing and long-term surface data.

To further explore the possibility that regional dynamics may lead to a coincidental moistening of the surface mixed layer with increasing aerosol independent of the aerosol radiative impact on

turbulence described above, a linear regression analysis was performed with the European Centre for Medium-Range Weather Forecasts (ECMWF) ERA-Interim reanalysis dataset (30). Table 1 shows the linear correlation between the daytime relative humidity at 1,000 hPa and the winds, divergence, static stability, and geopotential height from 7 y of February and March ECMWF data for the model grid cell located over the MCOH field station. The analysis shows that (*i*) 1,000 hPa relative humidity is not strongly correlated with any of the metrics examined, (*ii*) the strongest correlations are with the vertical velocity and divergence fields at 1,000 hPa and 750 hPa, and (*iii*) the differences in vertical velocity and divergence between more polluted conditions and less polluted conditions are small relative to the dynamic range of these quantities. These differences in zonal velocity, vertical velocity, and divergence, even if independent, together would explain only roughly 1–2% of the ~8% increase in relative humidity between more polluted and less polluted conditions. Furthermore, the vertical velocity and divergence parameters are neither independent of one another nor independent of the local turbulent dynamics in the boundary layer. These results do not suggest a strong dynamical effect related to the large-scale dynamics, at least in the ECMWF reanalysis, that might explain a coincidental increase in relative humidity in the surface mixed layer with the transport of BC aerosols to the location of the experiment. Nonetheless, further modeling is required to isolate the impact of aerosols from other meteorological impacts on surface mixed layer properties.

The shallow cumulus clouds observed over the northern Indian Ocean are embedded within a deep layer of BC aerosols. The response of boundary layer turbulence and clouds may depend on the vertical orientation of the absorbing aerosols relative to the cloud layer, as well as on the response of the clouds themselves. For example, in the Amazon region, where deeper cumulus clouds are embedded in absorbing BC aerosols, the introduction of BC aerosols in a model experiment reduced TKE below the aerosol layer and increased TKE in a narrow layer above the aerosol layer (31). At low aerosol amounts, increasing aerosol led to taller clouds, whereas at high aerosol amounts, increasing aerosol led to reduced cloudiness. In another model experiment, a reduction in latent heat flux from the surface due to high aerosol was sufficient to substantially reduce cloud cover (32). These results are broadly consistent with satellite observations over the Amazon (33).

The model-simulated reduction in TKE for the Amazon case is similar to our observations over the Indian Ocean; however, the increase in cloud depth over the Amazon for low aerosol amounts is considered a consequence of the microphysical impacts of aerosol on clouds, which is not likely to be a factor over the northern Indian Ocean. The mechanisms cited for invigoration of clouds by aerosols include suppression of rainfall and a related addition of latent heat from freezing of liquid drops. Even the cleanest clouds that we have observed are composed of drops that are too small to contribute to drizzle (3). Furthermore, the clouds are too shallow to contain ice. Simulated stratocumulus clouds with absorbing aerosol entirely above the cloud layer exhibited thickening due to reduced entrainment of dry air into the cloud layer at the cloud tops (9). TKE may in fact be enhanced in the boundary layer for absorbing aerosol above the stratocumulus clouds owing to the greater amount of condensed water in the overcast cloud layer. Nevertheless, entrainment is reduced because of the increased buoyancy of the aerosol layer above the cloud. Thus, the mechanism for thickening clouds over the southeastern Atlantic Ocean may be slightly different from the one we are proposing here for the northern Indian Ocean.

Suppression of boundary layer turbulence by BC aerosols can lead to additional impacts beyond changes in cloud radiative forcing. High relative humidity and large particle concentrations are related to low-visibility fog events (34), which have increased in frequency and duration over South Asia (35, 36). Furthermore, reduced vertical mixing and a lowering of the boundary layer top will increase the surface concentration of BC particles, which are known to have substantial negative impacts on human health in South Asia (37, 38).

ACKNOWLEDGMENTS. We thank Hung Nguyen for the expert project and flight management for CARDEX. The CARDEX campaign is supported by National Science Foundation Grant NSF-0721142 and was conducted by Scripps Institution of Oceanography with V. Ramanathan as the principal investigator. E.M.W. acknowledges support from the Desert Research Institute to participate in CARDEX, as well as from National Aeronautics and Space Administration Grant NNX11AG89G.

1. Ramanathan V, et al. (2007) Atmospheric brown clouds: Hemispherical and regional variations in long-range transport, absorption, and radiative forcing. *J Geophys Res* 112:D22S21.
2. Ramanathan V, et al. (2007) Warming trends in Asia amplified by brown cloud solar absorption. *Nature* 448(7153):575–578.
3. Roberts GC, Ramana MV, Corrigan C, Kim D, Ramanathan V (2008) Simultaneous observations of aerosol-cloud-albedo interactions with three stacked unmanned aerial vehicles. *Proc Natl Acad Sci USA* 105(21):7370–7375.
4. Twomey S (1977) The influence of pollution on the shortwave albedo of clouds. *J Atmos Sci* 34:1149–1152.
5. Albrecht BA (1989) Aerosols, cloud microphysics, and fractional cloudiness. *Science* 245(4923):1227–1230.
6. Ackerman AS, Kirkpatrick MP, Stevens DE, Toon OB (2004) The impact of humidity above stratiform clouds on indirect aerosol climate forcing. *Nature* 432(7020):1014–1017.
7. Stevens B, Feingold G (2009) Untangling aerosol effects on clouds and precipitation in a buffered system. *Nature* 461(7264):607–613.
8. Ackerman AS, et al. (2000) Reduction of tropical cloudiness by soot. *Science* 288(5468): 1042–1047.
9. Johnson BT, Shine KP, Forster PM (2004) The semi-direct aerosol effect: Impact of absorbing aerosols on marine stratocumulus. *Q J Roy Meteorol Soc* 130: 1407–1422.
10. Wilcox EM (2010) Stratocumulus cloud thickening beneath layers of absorbing smoke aerosol. *Atmos Chem Phys* 10:11769–11777.
11. Wilcox EM (2012) Direct and semi-direct radiative forcing of smoke aerosols over clouds. *Atmos Chem Phys* 12:139–149.
12. Koch D, Genio ADD (2010) Black carbon semi-direct effects on cloud cover: Review and synthesis. *Atmos Chem Phys* 10:7685–7696.
13. Ramanathan V, et al. (2011) Cloud Aerosol Radiative Forcing Dynamics EXperiment (CARDEX). ramanathan.ucsd.edu/files/CARDEX_prop_Jun_20.pdf. Accessed August 30, 2016.
14. Corrigan CE, Roberts GC, Ramana MV, Kim D, Ramanathan V (2008) Capturing vertical profiles of aerosols and black carbon over the Indian Ocean using autonomous unmanned aerial vehicles. *Atmos Chem Phys* 8:737–747.
15. Thomas R, et al. (2011) Measurement of turbulent water vapor fluxes using a lightweight unmanned aerial vehicle system. *Atmos Meas Tech* 4:5529–5568.
16. Lenschow DH, Stankov B (1986) Length scales in the convective boundary layer. *J Atmos Sci* 43(12):1198–1209.
17. Foken T (2008) *Micrometeorology* (Springer, Berlin), p. 306.
18. Brooks IM (2003) Finding boundary layer top: Application of a wavelet covariance transform to lidar backscatter profiles. *J Atmos Ocean Technol* 20:1092–1105.
19. Medeiros B, Nuijens L, Antoniazzi C, Stevens B (2010) Low-latitude boundary layer clouds as seen by CALIPSO. *J Geophys Res* 115:D23207.
20. Corrigan CE, Ramanathan V, Schauer JJ (2006) Impact of monsoon transitions on the physical and optical properties of aerosols. *J Geophys Res D Atmos* 111: D18208.
21. Ramanathan V, et al. (2001) Indian Ocean experiment: An integrated analysis of the climate forcing and effects of the great Indo-Asian haze. *J Geophys Res* 106: 28,371–28,398.
22. Heymsfield AJ, McFarquhar GM (2001) Microphysics of INDOEX clean and polluted trade cumulus clouds. *J Geophys Res* 106(D22):28653–28673.
23. Liu Z, et al. (2009) The CALIPSO lidar cloud and aerosol discrimination: Version 2 algorithm and initial assessment of performance. *J Atmos Ocean Technol* 26:1198–1213.
24. Winker DM, et al. (2009) Overview of the CALIPSO mission and CALIOP data processing algorithms. *J Atmos Ocean Technol* 26:2310–2323.
25. Pistone K, et al. (2016) Observed correlations between aerosol and cloud properties in an Indian Ocean trade cumulus regime. *Atmos Chem Phys* 16:5203–5227.
26. Norris J (2001) Has northern Indian Ocean cloud cover changed due to increasing anthropogenic aerosol? *Geophys Res Lett* 28:3271–3274.
27. Dey S, et al. (2011) Satellite-observed relationships between aerosol and trade-wind cumulus cloud properties over the Indian Ocean. *Geophys Res Lett* 38:L01804.
28. Kaufman YJ, Koren I (2006) Smoke and pollution aerosol effect on cloud cover. *Science* 313(5787):655–658.
29. Höpner FF, et al. (2016) Vertical profiles of optical and microphysical particle properties above the northern Indian Ocean during CARDEX 2012. *Atmos Chem Phys* 16:1045–1064.
30. Dee D, et al. (2011) The ERA-Interim reanalysis: Configuration and performance of the data assimilation system. *Q J R Meteorol Soc* 137(656):553–597.

31. Ten Hoeve JE, Jacobsen MZ, Remer LA (2012) Comparing results from a physical model with satellite and in situ observations to determine whether biomass burning aerosols over the Amazon brighten or burn off clouds. *J Geophys Res* 117:D08203.
32. Feingold G, Jiang H, Harrington J (2005) On smoke suppression of clouds in Amazonia. *Geophys Res Lett* 32(2):L02804.
33. Koren I, Martins JV, Remer LA, Afargan H (2008) Smoke invigoration versus inhibition of clouds over the Amazon. *Science* 321(5891):946–949.
34. Gautam R, Hsu NC, Kafatos M, Tsay S-C (2007) Influences of winter haze on fog/low cloud over the Indo-Gangetic plains. *J Geophys Res* 112:D05207.
35. Jenamani RK (2007) Alarming rise in fog and pollution causing a fall in maximum temperature over Delhi. *Curr Sci* 93(3):314–322.
36. Syed FS, Körnich KH, Tjernström M (2012) On the fog variability over south Asia. *Clim Dyn* 39:2993–3005.
37. Janssen NA, et al. (2011) Black carbon as an additional indicator of the adverse health effects of airborne particles compared with PM10 and PM2.5. *Environ Health Perspect* 119(12):1691–1699.
38. Smith KR (2000) National burden of disease in India from indoor air pollution. *Proc Natl Acad Sci USA* 97(24):13286–13293.